# Understanding of surface segregation of Cu and Zn on nano Si precipitates to the mechanical property improvement of high pressure die casting Al9Si3CuFe alloy

**DOI:**
10.1016/j.jallcom.2021.162219

**Document Version**
Accepted author manuscript

# Understanding of surface segregation of Cu and Zn on nano Si precipitates to the mechanical property improvement of high pressure die casting Al9Si3CuFe alloy

Yijie Zhang[a]*, Shihao Wang[a], Ewan Lordan[a], Kun Dou[b], Xiaorong Zhou[c],

Teruo Hashimoto[c]

[a]BCAST, Brunel University London, Uxbridge, Middlesex UB8 3PH, UK

[b]School of Metallurgy and Environment, Central South University, Changsha, 410083, China

[c]School of Materials, University of Manchester, Manchester M13 9PL, UK

*Corresponding author. Tel.: +441895268538; Fax: +441895269758; E-mail address: yijiezhang6@gmail.com.

## Abstract

To understand Si precipitation and its influence on mechanical property improvement in high pressure die casting (HPDC) Al9Si3CuFe alloy under direct ageing heat treatment, the precipitates in Al9Si3CuFe alloy containing *in-situ* $MgAl_2O_4$ particles is analyzed via atomic-resolution scanning transmission electron microscopy. It is shown that lath-like Si precipitates form in an average size of 50 nm in length, and a good orientation relationship of $\{010\}<001>_{Al}//\{111\}<01\text{-}1>_{Si}$ is observed between Si precipitate and matrix. Interestingly, Cu and Zn are observed to segregate onto Si/Al interface, which has a coarsening resisting effect on precipitate growth. The presence of these Si precipitates is the main factor contributing to the further improvement of mechanical properties of Al9Si3CuFe alloy, which results in an increase of 70 MPa in yield strength compared to the alloy without Si precipitates.

***Keywords***:

Si precipitate; Mechanical property; High pressure die casting; Al alloys

## 1. Introduction

Al alloys are widely used in automotive, aerospace and transport areas due to their excellent physical and mechanical properties, particularly in applications demanding high specific strength and corrosion resistance. Primary Al is typically produced via electrolysis in which ~16000 KWh of electricity is consumed to produce one ton of commercial purity Al — this amounts to approx.11 tons of $CO_2$ emissions [1], presenting a clear environmental issue. However, recycling Al alloys only requires 5% of the energy consumed in the production of primary Al, leading to significant reduction in $CO_2$ emissions (down to 0.3 $tCO_2$/tAl [2]). Considering the wide variety of commercial Al alloys (e.g. those based on Al-Si, Al-Mg, Al-Cu, Al-Mn, and Al-Zn [3]), it is very difficult to distinguish individual grades from the bulk mixture of recycled scraps. Due to these difficulties, impurities, such as Fe, are inevitable introduced into secondary alloys, degrading their quality. Therefore, it would be highly advantageous to produce secondary alloys which possess physical and mechanical properties that match or exceed their primary counterparts. This would not only present clear environmental benefits, but may also change the way we think about component design and manufacturing, with a circular economy in mind. Amongst these secondary alloys, Al9Si3CuFe alloy (LM24) is the most successful, possessing reasonable properties whilst maintaining a high tolerance of alloying elements. For example, LM24 can tolerate 7.5-9.5 % Si, 3-4 % Cu, Zn<3 %, Mg< 0.3%, Mn<0.5 %, Ni<0.5 %, and most importantly Fe<1.3 % (all in wt.%). Consequently, LM24 alloy is often used in high pressure die casting (HPDC), due to excellent casting properties and suitability for many engineering applications, including engine block, and transmission mounting brackets. Driven by an increasing demand for light weighting in the automotive industry, further improvement in mechanical properties of LM24 alloy are necessary to improve vehicle range and reduce $CO_2$ emissions.

For heat treatable AlSiCuMg alloys, precipitation strengthening is an important mechanisms for enhancing mechanical strength and involves the formation of nano-scale precipitates such as $Mg_5Si_6$ (β″) [4], $Al_2Cu$ (θ′) [5], $Al_5Cu_2Mg_8Si_6$ (Q′) [6]

and $Al_2CuMg$ (S) [7]. Since LM24 alloy already contains many alloying elements, the further adjustment of chemical elements has a limited influence on the mechanical properties. Strengthening can also be achieved through grain refinement, in which the addition of Al5Ti1B master alloy into the melt during casting has proven to be the most efficient grain refining method for Al alloys [8]. By combining the advantages from both Al and ceramic, particle reinforced metal matrix composites has been proven to improve both mechanical and physical properties via designed types of reinforcements, such as strength [9], modulus [10], damping capacity [11], thermal conductivity [12] and coefficient of thermal expansion [13]. Therefore, traditional methods for improving mechanical properties should be reconsidered, with innovations in material design and multiple strengthening mechanisms perhaps requiring inspiration from interdisciplinary research areas.

It has been reported that the use of *in-situ* nano particles, such as $TiB_2$ and $Al_2O_3$, as a reinforcement can improve the strength of Al-Si alloys via secondary phase dispersion strengthening and Orowan strengthening. When using particles as reinforcement in metal matrix composites, particle additions of at least 1 % are required to obtain a notable improvement in mechanical and physical properties. However, this improvement is accompanied by a decrease in elongation [9,14–16]. Elongation is an essential factor for Al alloys requiring fatigue strength and crash energy absorption, particularly when the alloy is intended for use in safety critical applications.

Recently, a patent related to a method and process to improve the mechanical properties of cast aluminium alloys [17] revealed that an introduction of $Al_2O_3$, TiC and $TiB_2$ particles less than 0.5 % benefits to an improvement in both tensile strength and elongation of Al alloys. And $MgAl_2O_4$ was reported it could be a potent nucleation substrate for α-Al due to a small misfit of approx. 1.4 % and a good orientation relationship of (111)[110]$MgAl_2O_4$ // (111)[110]Al between $MgAl_2O_4$ and Al [18–20]. Hence, it could be a potential approach used for Al alloys to improve strength and elongation simultaneously via grain refinement strengthening, secondary phase dispersion strengthening and Orowan strengthening.

In our previous study [21], the elongation of HPDC A380 alloy increased from 4.9% to 5.4% following the addition of *in-situ* $Mg_2AlO_4$ particles as grain refiner—the variability in elongation and yield strength was also reduced. With direct aging treatment for HPDC LM24 alloy containing *in-situ* $MgAl_2O_4$ particles [22], a significant improvement of tensile strength is achieved whilst maintaining the elongation of the base alloy. However, the precipitation strengthening mechanism in LM24 alloy having *in-situ* $MgAl_2O_4$ particles is not fully understood.

Basing on understanding of *in-situ* $MgAl_2O_4$ particles in LM24 alloy, in the present study, the precipitates are investigated via analytical transmission electron microscopy and aberration corrected transmission electron microscopy aiming to reveal their characteristics to further understanding of strengthening mechanism for enhanced mechanical properties.

## 2. Experimental methods

LM24 alloy consisting of 8.09 % Si, 3.11 % Cu, 1.78 % Zn, 0.86 % Fe, 0.22 % Mn, 0.16 % Mg and 0.04 % Ti, supplied by Norton UK, was used in this study. To synthesis *in-situ* $MgAl_2O_4$ particles in the melt (LM24-M), melt conditioning treatment via a rotor-stator high shear device was employed at a speed of 1500 rpm

for 30 minutes at 725±5 ºC [21,22]. The melt was then degassed using a commercial rotary degassing unit for 8 min at 350 rpm rotation speed with an Ar flow rate of 4 L/min. The purified melt was then manually poured into shot sleeve of a Frech 4500 kN locking force cold chamber HPDC machine, to produce tensile samples (gauge diameter: 6.35 mm). The pouring temperature of melt, die temperature and shot sleeve temperature were 680±5 ºC, 200±5 ºC and 180±5 ºC, respectively. For comparison, LM24 alloy samples were produced using the same parameters but without high shear melt conditioning. After stabilization at room temperature for 24 hours, a group of the tensile samples underwent direct ageing at 155±5 ºC for 15 hours (T5). Considering a super-saturated α-Al is attained due to the high cooling rates (500~1000 K/s) in HPDC solidification, T5 is a potential heat treatment to improve the mechanical properties of HPDC components via precipitation strengthening. This approach avoids the residual stresses induced by water quenching at a high temperature (490 ~ 540°C), which is a solutionizing and quenching process adopted in traditional T6 heat treatment. Tensile testing was carried out on an Instron 5500 Universal electromechanical testing system at ambient temperature. A 50 mm extensometer was used to record tensile data, with a ramping rate of 1mm/min. Eight samples were tested in each condition to obtain the average tensile properties.

Samples for metallographic characterization were prepared according to standard procedures. Foils for transmission electron microscopy (TEM) were mechanically ground and punched into 3 mm diameter discs, followed by manual polishing down to 80-100 μm thickness. The final thinning was done by twin-jet electro polishing using a 30 % nitric acid/70 % methanol (vol.%) solution and chilled to −30°C. A potential of 15 V was used for electro polishing yielding excellent results. Prior to TEM analysis the samples were cleaned by dual beam plasma ion polishing (PIPS) to further improve the quality of electron-transparent regions. Conventional bright field (BF) TEM imaging and high-resolution transmission electron microscopy (HRTEM) imaging were performed on a JEOL 2100F instrument operated at an accelerating voltage of 200 kV. Atomic resolution high-angle annular dark-field (HAADF) STEM imaging was carried out in a Titan G2 80-200 S/TEM instrument operated at 200 kV. Chemical analyses were performed in-situ using ChemiSTEM™ technology, employing four annular silicon drift detectors (SDD) offering high sensitivity energy dispersive spectrometry (EDS).

## 3. Results

### 3.1 Mechanical properties

Fig.1 shows the mechanical properties of LM24 alloy with and without *in-situ* $MgAl_2O_4$ under T5 treatment. Comparing properties in the as-cast state, with T5 heat treatment an increase in tensile strength is obtained for both LM24 and LM24-M alloy [22], which is well agreed with the improvement for A380 alloy reported by Lumley et al [23]. For LM24 alloy without *in-situ* $MgAl_2O_4$ particles and A380 alloy, after T5 treatment an improvement of 75 MPa and 62 MPa in yield strength (YS) is obtained, respectively. Whilst with *in-situ* $MgAl_2O_4$ particles, an increasing of 128 MPa is achieved for T5-treated LM24-M alloy. Such improvements are very similar to the increase of 154 MPa observed for Al9Si3.5Cu alloy having 0.1 % Mg after full heat

treatment of solution at 510 ºC for 30 min and ageing at 170 ºC for 24 hours (T6) previously reported by Yang et al. [24].

Unfortunately, a decrease in elongation is observed after T5 treatment not only in LM24 alloy but also in A380 alloy, and even in Al9Si3.5Cu alloy with T6 treatment, as shown in Fig. 1. After heat treatment, the elongation decreased by 1.3 %, 0.5 %, 2 % and 0.8 % for LM24-T5, LM24-M-T5, A380-T5 and Al9Si3Cu-T6, respectively. This is a normal phenomenon in precipitation strengthening: an increasing in strength is accompanied by a decrease in elongation, and vice versa. Hardness measurements provide a rough estimate of the relationship between precipitates and strength [6,25]. High levels of hardness indicate high strength and low elongation. More accurate techniques, such as TEM observation, allow one to visualize and analyze precipitates.

### 3.2 Precipitates

Normally, θ′ and Q′ are the dominant kinds of precipitates contributing to strength improvement for LM24 alloy after heat treatment [23,24]. However, Q′ phase is not found in HPDC LM24 alloy with the introduction of *in-situ* $MgAl_2O_4$ [22]. Regarding EDS mapping and HRTEM image, the possible types of precipitates for LM24-M alloy after T5 treatment are $Al_2Cu$ (θ′) (Fig.2b,d) and Si (Fig.2e). The appearance of Si precipitates is discussed in our previous study [22] and is trigged by the increased dislocation density caused by the *in-situ* $MgAl_2O_4$ particles. Two types of Si precipitates, sphere Si and lath-like Si, are observed in present study, where sphere Si is the same as that reported by Li et al [26]. Interestingly, a bright layer is observed on the Si/Al interface (Fig.2a), which indicates that element segregation occurs where the element atomic number is higher than Si. EDS maps confirmed that the segregation elements are Cu (Fig.2f) and Zn (Fig.2g).

The morphology of Si precipitates and the orientation relationship (OR) between Si precipitate and Al matrix is shown in Fig. 3. With an incident beam parallel to $<001>_{Al}$, the morphology of Si precipitates viewed from different zone axes is revealed in Fig. 3a. For illustrating the different shape observed in Fig.3a, three types of projected morphology on image plane of Si precipitates in Al matrix are schematically portrayed in Fig. 3b, with their projections shown along the beam direction. Fig. 3c,e and Fig. 3d,f show the HRTEM images of two types of Si precipitates with the beam direction parallel to $<011>_{Si}$ and $<211>_{Si}$ , respectively. Identification of the Si precipitates can be confirmed after indexing the lattice parameters of (011)Al as an internal reference to ensure the accuracy of the measurement in Fig. 3e,f. In addition, the habit plane for Si precipitate is identified as $\{111\}_{Si}$ that is parallel to {010}Al, at which an OR can also be recognized with the adjacent Al matrix: $\{111\}<01\text{-}1>_{Si}$ // $\{010\}<001>_{Al}$. The OR between Si and Al matrix is in agreement with the results reported by Mørtsell et al. [27]. The third type of Si precipitates viewing along $<111>_{Si}$ is presented in Fig. 4. In consistency with the morié fringes found in Fig. 3a, the spacing between fringes is 3.7 nm as well (Fig. 4a,b). According to the identified OR, translation morié fringes is created under such viewing direction, being the result of overlapping of $\{020\}_{Al}$ and $\{022\}_{Si}$, as shown in Fig.4c.

## 4. Discussion

### 4.1 Segregation on Si precipitates

To identify segregation elements on the Si precipitate/Al interface, HAADF images and EDS maps were carried with a beam parallel to $<001>_{Al}$ in Fig. 5a and $<011>_{Al}$ in Fig. 5b, respectively. Along $<001>_{Al}$ direction, Si precipitate shows as an edge-on projection along $<011>_{Si}$, with the whole Si/Al interface is surrounded by Cu and Zn elements, as seen in Fig. 5a. While under the viewing direction along $<110>_{Al}$, thickness of the Si precipitates is not uniform along the length direction (Fig. 5b). As shown in Fig. 6, the thickness maximized at the center position and decays towards two ends, which is coincide with the intensity variation in the Si map. As compared to Fig. 5a, the Cu and Zn segregation (Fig.5b) at two ends is less distinguished due to the variation in thickness. This does not mean that there is really less segregation at two ends of the Si precipitate, as illustrated in insert sketch in Fig.6. In fact, the 'reduced' segregation is actually a visual effect due to the precipitate viewed from a non-edge-on direction, under which it shows a faded edge along with a decay thickness and the returned signal is too weak to identify all segregation elements during EDS acquisition.

For binary Al-Si alloy, it is reported that Si usually precipitate on $\{111\}_{Al}$ [29] which having an incoherent Si/Al interface. Whilst with elemental segregation on Si precipitate [27], it tends to precipitate on $\{010\}_{Al}$ leading to form a semi-coherence interface instead. The presence of segregation seems acting as a misfit reliever [30], and suppressing misfit dislocation at the interface [31].

### 4.2 Mechanical improvement

Compared with a YS of 222±3 MPa in LM24 alloy, a further improvement of 75 MPa is obtained in LM24-M alloy (297±5 MPa), as seen in Fig.1. Since the only difference between LM24 and LM24-M is the presence of *in-situ* $MgAl_2O_4$ particles, this improvement is likely attributed to microstructure modification, such as grain refinement and precipitates, which are both influenced by the introduction of *in-situ* particles. Considering the experimental findings presented in this study and the results reported previously [22–24], the observed improvement in mechanical properties of LM24 alloy with T5 treatment is similar to that obtained after full heat treatment (T6). By using T5 instead of T6, it not only benefits from avoiding component distortion during the quenching process but also saves energy by skipping the solution process, which occurs at high temperature.

#### 4.2.1 Mechanical property enhanced by Si precipitates

In the present study, this is the first time Si precipitates having Cu and Zn segregation are observed in Al9Si3CuFe alloy. Li et al. [26] show that 70 nm Si precipitates can result in a 79 MPa increase in tensile strength for a selective laser melted *in-situ* $TiB_2$/AlSi10Mg composite where a super saturation of about 2.5 % Si obtained due to the high cooling rates of $10^3$~$10^5$K/s encountered in the selective laser melting process. A similar nano Si precipitate was found in Al-Si alloy with high pressure solution heat treatment up to 6 GPa that aims to achieve supersaturated Si in α-Al after ageing at 150 ºC [32]. In reference [32], Si precipitates with a length of 50-100

nm and a thickness of 5-20 nm were obtained and a cube-cube identical orientation relationship between Si precipitate and matrix was observed.

At equilibrium solidification, the maximum solute solubility of Si in Al is approx. 1.65 % at 577ºC [33]. The Orowan-Ashby equation is given by [34,35]:

$$\Delta\sigma_{Orowan} = \frac{0.4MGb\ln(\frac{\sqrt{2/3}dp}{b})}{\pi\sqrt{2/3}dp(\sqrt{\pi/4V_P}-1)\sqrt{1-\upsilon}} \quad (1)$$

Where M is the Taylor factor (~3.06 for Al), G is shear modulus (~25.4 GPa for Al matrix), b is the Burgers vector (~0.286 nm for Al), $\upsilon$ is the Poisson's ratio (~0.3 for Al), $V_p$ is the volume fraction of precipitate. According to equation (1), Si precipitates having average size ($d_p$) of 50 nm caused by 1.65 % of supersaturation could contribute an increase of 70 MPa in YS of LM24-M alloy with T5 treatment. This suggests that the 75 MPa improvement in YS of LM24-M alloy (T5 condition) compared to YS of LM24 alloy (T5 condition) is mainly due to the existence of Si precipitates.

Considering the size of Si precipitate with interfacial segregation is smaller than that without interfacial segregation, and the improvement in tensile properties of LM24 alloy is caused by the presence of Si precipitates, it seems that this kind of interface segregation inhibits precipitate growth during ageing [27], which enhances tensile properties via Orowan strengthening [36]. A similar coarsening-resisting effect of interfacial segregation on the precipitate is reported by Booth-Morrison [37] and Marquis [38], where Zr segregation onto $Al_3$(Sc,Zr) precipitate and Mg segregation onto $Al_3Sc$ precipitate surface where respectively observed. The segregation of solute to these interfaces may produce intermediate interfacial states that affect precipitate growth and morphology [39], which results in an incremental increase in strength [37].

### 4.2.2 Mechanical property improved by grain refinement

It has been proved by Wang et al [19], Li et al [20] and Zhang et al [21] that *in-situ* $MgAl_2O_4$ particle produced by high shear melt conditioning can promote grain refinement of Al alloys. Considering high cooling rates promote grain refinement, several researchers have reported that an average grain size of about 10 μm and 17.5 μm could be obtained for Al7Si0.3Mg (A356) alloy [40] and Al9Si0.6Mg0.6Mn alloy [15], respectively. In the present study, grain refinement of α-Al was observed in both the edge and center regions of the tensile sample following the introduction of *in-situ* $MgAl_2O_4$ particles, with an average grain size of 20 μm and 10 μm reported for LM24 and LM24-M alloy respectively (Fig. 7). According to the Hall-Petch equation $\Delta\sigma = kd^{-1/2}$, there is a ~3 MPa increase in YS when grain size decreases from 20 μm to 10 μm, where *k* is constant and typically equal to 40 MPa/$\mu m^{1/2}$ for Al alloy [34,40]. This indicates that grain refinement is not the main factor contributing to the observed improvement in YS. The main advantage of grain refinement in HPDC alloys is the improvement in mechanical properties variation due to defect reduction and uniform secondary phase dispersion [21]; such defects adversely affect the variability in mechanical properties.

## 5. Conclusions

In summary, in-situ $MgAl_2O_4$ particles can promote the formation of nano Si precipitates that have a good orientation relationship of $\{010\}<001>_{Al}//\{111\}<01\text{-}1>_{Si}$ with matrix in HPDC LM24 alloy following direct ageing treatment. For the first time, interfacial segregation of Cu and Zn on Si precipitates has been observed. Such kind of segregation has a coarsening-resisting effect on precipitate growth, and contributes to an increase of approx. 70 MPa in yield strength for the studied alloy. The presence of Zn in LM24 alloy does not form any intermetallic phase, rather it segregates onto the Si precipitate/Al interface.

## Acknowledgements

This project is financially supported by EPSRC UK in the EPSRC Centre for Innovative Manufacturing in Liquid Metal Engineering (The EPSRC Centre—LiME).

## Competing interests

The author(s) declare no competing interests.

## Data availability

The datasets generated and analyzed during the current study are available from the corresponding author on reasonable request.

## References

[1] T. Peng, X. Ou, X. Yan, G. Wang, Life-cycle analysis of energy consumption and GHG emissions of analysis of energy consumption GHG aluminium production in China, Energy Procedia. 158 (2019) 3937–3943. https://doi.org/10.1016/j.egypro.2019.01.849.

[2] J.A. Moya, A. Boulamati, S. Slingerland, R. Van Der Veen, M. Gancheva, K.M. Rademaekers, J.J.P. Kuenen, A.J.H. Visschedijk, Energy Efficiency and GHG Emissions: Prospective Scenarios for the Aluminium Industry, 2015. https://doi.org/10.2790/263787.

[3] J.R. Davis, Aluminum and Aluminum Alloys, in: J.. Davis (Ed.), Alloy. Underst. Basics, ASM International, 2001: pp. 351–416. https://doi.org/10.1361/autb2001p351.

[4] S.H. Wang, C.H. Liu, J.H. Chen, X.L. Li, D.H. Zhu, G.H. Tao, Hierarchical nanostructures strengthen Al-Mg-Si alloys processed by deformation and aging, Mater. Sci. Eng. A. 585 (2013) 233–242. https://doi.org/10.1016/j.msea.2013.07.061.

[5] C. Liu, S.K. Malladi, Q. Xu, J. Chen, F.D. Tichelaar, X. Zhuge, H.W. Zandbergen, In-situ STEM imaging of growth and phase change of individual

CuAlX precipitates in Al alloy, Sci. Rep. 7 (2017) 1–8. https://doi.org/10.1038/s41598-017-02081-9.

[6] X. Dong, H. Yang, X. Zhu, S. Ji, High strength and ductility aluminium alloy processed by high pressure die casting, J. Alloys Compd. 773 (2019) 86–96. https://doi.org/10.1016/j.jallcom.2018.09.260.

[7] M.J. Styles, C.R. Hutchinson, Y. Chen, A. Deschamps, T.J. Bastow, The coexistence of two S ($Al_2CuMg$) phases in Al-Cu-Mg alloys, Acta Mater. 60 (2012) 6940–6951. https://doi.org/10.1016/j.actamat.2012.08.044.

[8] Y. Zhang, S. Ji, Z. Fan, Improvement of mechanical properties of Al-Si alloy with effective grain refinement by in-situ integrated Al2.2Ti1B-Mg refiner, J. Alloys Compd. 710 (2017) 166–171. https://doi.org/10.1016/j.jallcom.2017.03.244.

[9] H. Yi, N. Ma, X. Li, Y. Zhang, H. Wang, High-temperature mechanics properties of in situ $TiB_2$ reinforced Al-Si alloy composites, Mater. Sci. Eng. A. 419 (2006) 12–17. https://doi.org/10.1016/j.msea.2005.10.020.

[10] S. Amirkhanlou, Y. Zhang, S. Ji, Z. Fan, Young's Modulus of Al–Si–Mg–Cu based alloy under different heat treatment processes, Miner. Met. Mater. Ser. (2017) 335–342. https://doi.org/10.1007/978-3-319-51541-0_44.

[11] Y. Zhang, N. Ma, H. Wang, Y. Le, S. Li, Effect of Ti and Mg on the damping behavior of in situ aluminum composites, Mater. Lett. 59 (2005) 3775–3778. https://doi.org/10.1016/j.matlet.2005.06.055.

[12] O. El-Kady, A. Fathy, Effect of SiC particle size on the physical and mechanical properties of extruded Al matrix nanocomposites, Mater. Des. 54 (2014) 348–353. https://doi.org/10.1016/j.matdes.2013.08.049.

[13] N.K. Sharma, R.K. Misra, S. Sharma, Modeling of thermal expansion behavior of densely packed Al/SiC composites, Int. J. Solids Struct. 102–103 (2016) 77–88. https://doi.org/10.1016/j.ijsolstr.2016.10.015.

[14] Y. Zhang, N. Ma, H. Wang, Improvement of yield strength of LM24 alloy, Mater. Des. 54 (2014) 14–17. https://doi.org/10.1016/j.matdes.2013.08.026.

[15] X. Dong, H. Youssef, Y. Zhang, H. Yang, S. Wang, S. Ji, Advanced heat treated die-cast aluminium composites fabricated by $TiB_2$ nanoparticle implantation, Mater. Des. 186 (2020) 108372. https://doi.org/10.1016/j.matdes.2019.108372.

[16] Y. Wu, J. Zhang, H. Liao, G. Li, Y. Wu, Development of high performance near eutectic Al-Si-Mg alloy profile by micro alloying with Ti, J. Alloys Compd. 660 (2016) 141–147. https://doi.org/10.1016/j.jallcom.2015.11.083.

[17] Y. Zhang, S. Ji, Y. Wang, Methods and process to improve the mechanical properties of cast aluminium alloys at ambient temperature and at elevated temperatures, WO 2018/142141 A1, 2018.

[18] D. Zhang, L. Wang, M. Xia, N. Hari Babu, J.G. Li, Misfit paradox on nucleation potency of MgO and $MgAl_2O_4$ for Al, Mater. Charact. 119 (2016) 92–98. https://doi.org/10.1016/j.matchar.2016.07.018.

[19] Y. Wang, H. Li, Z. Fan, G. Scamans, Characterisation of Oxide Films in Al-Mg Alloy Melts, Mater. Sci. Forum. 765 (2013) 220–224. https://doi.org/10.4028/www.scientific.net/MSF.765.220.

[20] H.T. Li, Y. Wang, Z. Fan, Mechanisms of enhanced heterogeneous nucleation during solidification in binary Al-Mg alloys, Acta Mater. 60 (2012) 1528–1537. https://doi.org/10.1016/j.actamat.2011.11.044.

[21] Y. Zhang, J.B. Patel, J. Lazaro-Nebreda, Z. Fan, Improved Defect Control and Mechanical Property Variation in High-Pressure Die Casting of A380 Alloy by High Shear Melt Conditioning, JOM. 70 (2018) 2726–2730. https://doi.org/10.1007/s11837-018-3005-y.

[22] Y. Zhang, S. Wang, E. Lordan, Y. Wang, Z. Fan, Improve mechanical properties of high pressure die cast Al9Si3Cu alloy via dislocation enhanced precipitation, J. Alloys Compd. 785 (2019) 1015–1022. https://doi.org/10.1016/j.jallcom.2019.01.278.

[23] R.N. Lumley, R.G. Odonnell, D.R. Gunasegaram, M. Givord, Heat treatment of high-pressure die castings, Metall. Mater. Trans. A. 38 (2007) 2564–2574. https://doi.org/10.1007/s11661-007-9285-4.

[24] H. Yang, S. Ji, W. Yang, Y. Wang, Z. Fan, Effect of Mg level on the microstructure and mechanical properties of die-cast Al-Si-Cu alloys, Mater. Sci. Eng. A. 642 (2015) 340–350. https://doi.org/10.1016/j.msea.2015.07.008.

[25] X. Dong, X. Zhu, S. Ji, Effect of super vacuum assisted high pressure die casting on the repeatability of mechanical properties of Al-Si-Mg-Mn die-cast alloys, J. Mater. Process. Technol. 266 (2019) 105–113. https://doi.org/10.1016/j.jmatprotec.2018.10.030.

[26] X.P. Li, G. Ji, Z. Chen, A. Addad, Y. Wu, H.W. Wang, J. Vleugels, J. Van Humbeeck, J.P. Kruth, Selective laser melting of nano-$TiB_2$ decorated AlSi10Mg alloy with high fracture strength and ductility, Acta Mater. 129 (2017) 183–193. https://doi.org/10.1016/j.actamat.2017.02.062.

[27] E.A. Mørtsell, F. Qian, C.D. Marioara, Y. Li, Precipitation in an A356 foundry alloy with Cu additions - A transmission electron microscopy study, J. Alloys Compd. 785 (2019) 1106–1114. https://doi.org/10.1016/j.jallcom.2019.01.229.

[28] A.M. Cassell, J.D. Robson, X. Zhou, T. Hashimoto, M. Besel, The direct observation of copper segregation at the broad faces of η′ and η precipitates in AA7010 aluminium alloy, Mater. Charact. 163 (2020) 110232. https://doi.org/10.1016/j.matchar.2020.110232.

[29] F. Lasagni, B. Mingler, M. Dumont, H.P. Degischer, Precipitation kinetics of Si

in aluminium alloys, Mater. Sci. Eng. A. 480 (2008) 383–391. https://doi.org/10.1016/j.msea.2007.07.008.

[30] M. Liu, R. Zheng, W. Xiao, X. Yu, Q. Peng, C. Ma, Concurrent enhancement of strength and ductility for Al-Si binary alloy by refining Si phase to nanoscale, Mater. Sci. Eng. A. 751 (2019) 303–310. https://doi.org/10.1016/j.msea.2019.02.081.

[31] T. Saito, F.J.H. Ehlers, W. Lefebvre, D. Hernandez-Maldonado, R. Bjørge, C.D. Marioara, S.J. Andersen, E.A. Mørtsell, R. Holmestad, Cu atoms suppress misfit dislocations at the β″/Al interface in Al-Mg-Si alloys, Scr. Mater. 110 (2016) 6–9. https://doi.org/10.1016/j.scriptamat.2015.07.033.

[32] M. Liu, H. Fu, L. Tian, W. Xiao, Q. Peng, C. Ma, Nucleation and growth mechanisms of nano-scaled Si precipitates in Al-7Si supersaturated solid solution, Mater. Des. 121 (2017) 373–382. https://doi.org/10.1016/j.matdes.2017.02.082.

[33] P. Rambabu, N. Eswara Prasad, V. V Kutumbarao, R.J.H. Wanhill, Aluminium Alloys for Aerospace Applications, in: N. Eswara Prasad, R.J.H. Wanhill (Eds.), Aerosp. Mater. Mater. Technol. Vol. 1 Aerosp. Mater., 1st ed., Springer Singapore, 2017: pp. 29–52. https://doi.org/10.1007/978-981-10-2134-3.

[34] S. Amirkhanlou, S. Ji, Y. Zhang, D. Watson, Z. Fan, High modulus Al-Si-Mg-Cu/$Mg_2Si$-$TiB_2$ hybrid nanocomposite: Microstructural characteristics and micromechanics-based analysis, J. Alloys Compd. 694 (2017) 313–324. https://doi.org/10.1016/j.jallcom.2016.10.016.

[35] Z. Zhang, D.L. Chen, Contribution of Orowan strengthening effect in particulate-reinforced metal matrix nanocomposites, Mater. Sci. Eng. A. 483–484 (2008) 148–152. https://doi.org/10.1016/j.msea.2006.10.184.

[36] Q. Wang, Z. Li, S. Pang, X. Li, C. Dong, P.K. Liaw, Coherent precipitation and strengthening in compositionally complex alloys: A review, Entropy. 20 (2018) 1–23. https://doi.org/10.3390/e20110878.

[37] C. Booth-Morrison, D.C. Dunand, D.N. Seidman, Coarsening resistance at 400 °C of precipitation-strengthened Al-Zr-Sc-Er alloys, Acta Mater. 59 (2011) 7029–7042. https://doi.org/10.1016/j.actamat.2011.07.057.

[38] E.A. Marquis, D.N. Seidman, M. Asta, C. Woodward, V. Ozolins, Mg Segregation at Al/$Al_3Sc$ Heterophase Interfaces on an Atomic Scale: Experiments and Computations, Phys. Rev. Lett. 91 (2003) 36101. https://doi.org/10.1103/PhysRevLett.91.036101.

[39] L. Bourgeois, C. Dwyer, M. Weyland, J.F. Nie, B.C. Muddle, Structure and energetics of the coherent interface between the θ′ precipitate phase and aluminium in Al-Cu, Acta Mater. 59 (2011) 7043–7050. https://doi.org/10.1016/j.actamat.2011.07.059.

[40] Y. Zhang, E. Lordan, K. Dou, S. Wang, Z. Fan, Influence of porosity characteristics on the variability in mechanical properties of high pressure die casting (HPDC) AlSi7MgMn alloys, J. Manuf. Process. 56 (2020) 500–509. https://doi.org/10.1016/j.jmapro.2020.04.071.

**Figure captions**

Figure 1 An improvement of tensile strength in LM24 and LM24-M alloys after T5 direct ageing treatment is obtained whilst a slight decrease in elongation occurs to these two kinds of alloys. The same trend of property before and after heat treatment has been reported for A380 alloy in the T5 condition [23], and for Al9Si3Cu alloy following T6 treatment [24].

Figure 1

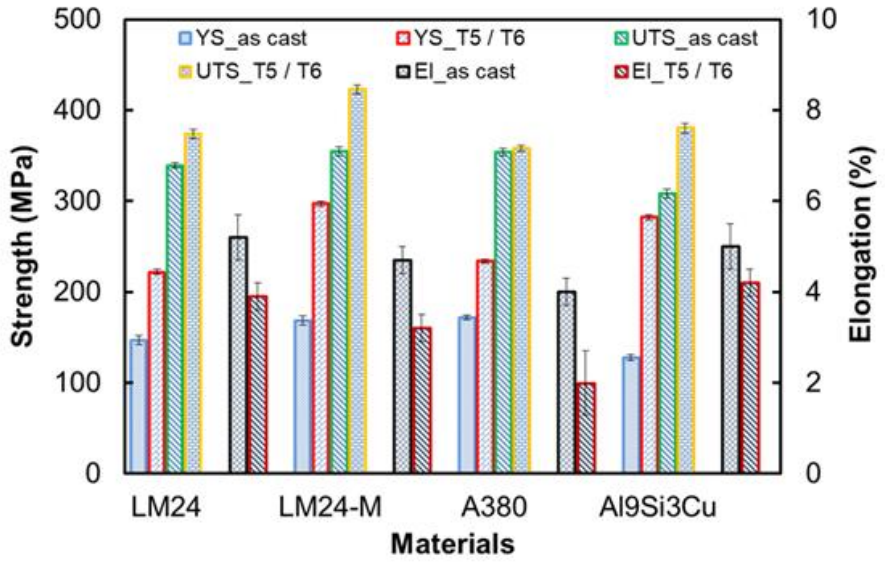

Figure 2 STEM HAADF and EDS analysis of θ′ and Si precipitates in LM24-M alloy after direct aging treatment. (a) Low-mag HAADF STEM image showing the co-existence of θ′ and Si precipitates; (b, c, d) EDS map of the θ′ precipitate marked in (a) and the corresponding atomic resolution HAADF STEM image; (d-g) HAADF STEM image of the labelled Si precipitate in (a) and the corresponding EDS maps of Si (e), Cu (f), Zn (g) and Mg (h). The brightness at the Si/Al interface indicates segregation of elements with a higher atomic number than Si. EDS confirmed that the segregation elements are Cu (f) and Zn (g).

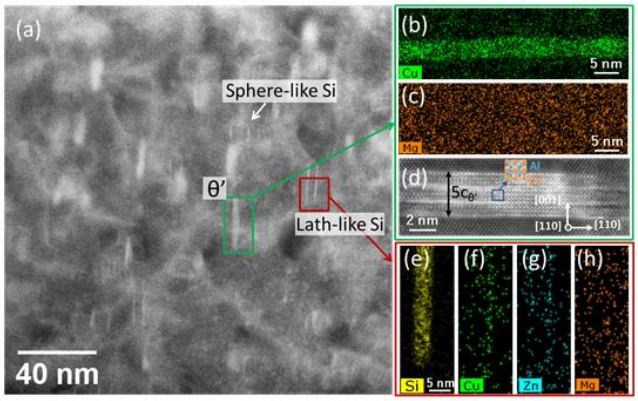


Figure 3 TEM analysis of Si precipitates. (a) Bright-field TEM image showing the morphology of Si precipitates viewed from different zone axes. (b) Sketch map showing Si precipitates in the Al matrix and their outcome shapes observed on the projection plane. (c-f) HRTEM images of Si precipitates of the type 1 (c, e) and type 2 (d, f) indicated in (a). The habit plane of {111}Si is identified for Si precipitates, which has an OR with Al: {111}<01-1>Si // {010}<001>Al.

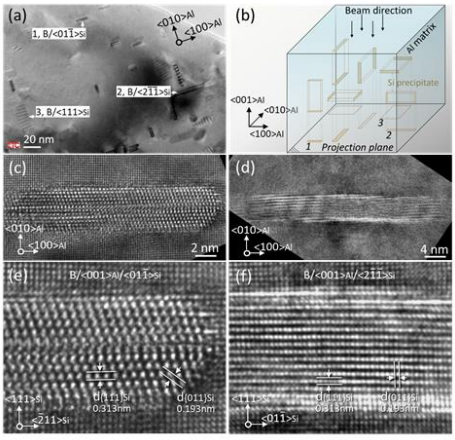

Figure 4 (a,b) HRTEM images showing a Si precipitate of type 3 in Figure 3a, and (c) analysis of translation morié fringe when {111}Si is overlapped with {100}Al under the OR of {111}<01-1>Si // {010}<001>Al.

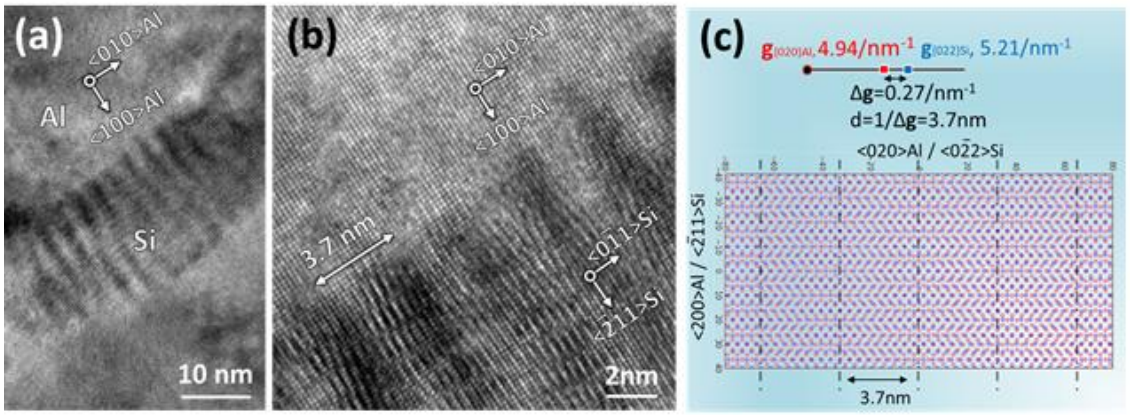


Figure 5 HAADF images and the corresponding EDS maps acquired along beam direction parallel to (a) <001>Al and (b) <011>Al. A edge-on projection of the lath-like Si precipitate is obtained in (a). While as tilted 45 degrees from the zone axis in (a), the precipitate in (b) in no uniform in thickness along the length direction, maximum thickness occurs at the center and decays towards two sides. The geometry effect (decaying thickness) destroys the segregation layer on the end of two sides.

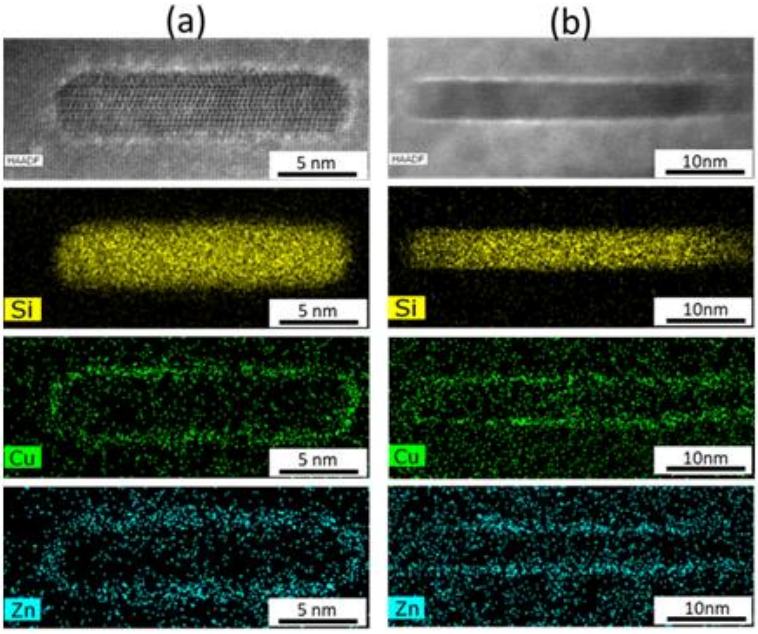

Figure 6 HAADF STEM images and the corresponding EDS maps acquired along beam directions parallel to (a) <001>Al and (b) <011>Al, respectively. An edge-on projection of the lath-like Si precipitate is obtained in (a). While as tilted 45 degrees from the zone axis in (a), the precipitate in (b) in no uniform in thickness along the length direction, maximum thickness occurs at the center and decays towards two sides. The geometry effect (decaying thickness) prevent of visualization of the segregation layer towards the end of two sides.

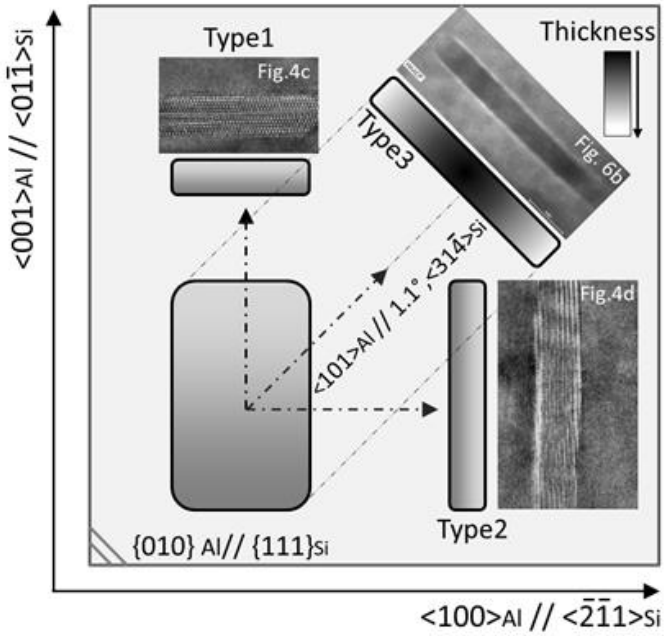


Figure 7 A good grain refinement of α-Al in both edge and center area of tensile sample obtains with addition of in-situ $MgAl_2O_4$ particles, and an average grain size of 20 μm and 10 μm is achieved for LM24 and LM24-M alloy respectively.